CrystEngComm

Dynamic Article Links

Cite this: *CrystEngComm*, 2012, **14**, 3103

www.rsc.org/crystengcomm

PAPER

Sonocrystallization of zeolitic imidazolate frameworks (ZIF-7, ZIF-8, ZIF-11 and ZIF-20)†

Beatriz Seoane,[a] Juan M. Zamaro,[b] Carlos Tellez[a] and Joaquin Coronas*[a]

Received 17th October 2011, Accepted 7th February 2012
DOI: 10.1039/c2ce06382d

Zeolitic imidazolate frameworks ZIF-7, ZIF-8, ZIF-11 and ZIF-20 have been synthesized by sonocrystallization. In general, crystals obtained at lower temperatures and shorter times are smaller and have a narrower size distribution than those achieved by conventional solvothermal synthesis. Moreover, crystallization curves have been calculated from the XRD patterns and the Gualtieri's model has been applied to simulate the extent of crystallization as a function of time. According to the parameters calculated, for ZIF-8 the nucleation rate controls the synthesis reaction, while for ZIF-11 and ZIF-20 both growth and nucleation rates are similar.

Introduction

Metal–organic frameworks (MOFs) are porous solids composed of inorganic units of metal or metal clusters connected by organic linkers forming a three dimensional skeleton.[1–3] MOFs are usually obtained by solvothermal synthesis using conventional heating (ST),[4] although recently microwave (MOF-5,[5–7] MIL-53,[8] MIL-101[8] and ZIF-8[9]), electrochemical[10] and ultrasound (US) (MOF-5[11] and HKUST-1[12,13]) methods have been investigated. MOFs have found application, among others, in adsorption,[14] catalysis,[15] membrane separation,[9,16] encapsulation,[17] sensing[18] and drug delivery.[19]

US synthesis is useful for obtaining different types of nanomaterials due to the localized extremely high temperatures (5000 K) and pressures (1800 atm) caused by cavitation of the liquid medium.[20,21] By means of ultrasounds, pure phases of zeolitic materials have been successfully synthesized.[22–24] However, the use of ultrasounds for the synthesis of MOFs is a little explored area, still virtually unknown in relation to the so-called zeolitic imidazolate frameworks (ZIFs). The sonocrystallization has been reported for MOF-5,[11] HKUST-1,[13] MIL-53[25] and nanosheets of a fluorescent MOF with the $[Zn(BDC)(H_2O)]_n$ formula (BDC = 1,4 benzenedicarboxylate).[12]

ZIFs are a subclass of MOFs which have an exceptionally high chemical and thermal stability.[26] In particular, ZIF-7 and ZIF-8, ZIF-11 and ZIF-20 are materials with the zeolitic-type topologies SOD, RHO and LTA, respectively.[26,27] Herein we demonstrate the sonochemical synthesis or sonocrystallization of these four ZIFs. The ultrasound syntheses of ZIFs were carried out with the same molar proportions of reactants as those reported in ST protocols.[26,27] In addition, the motivation of this work is not only related to gain insight into the sonocrystallization of ZIFs but also to the possibility of producing crystalline materials with a narrower particle size distribution. Among other fields of application, this has tremendous importance in the preparation of the so-called mixed matrix membranes with special fillers (those promoting synergy with membrane polymers),[28] in which MOFs are included as we have previously studied.[16,29,30]

Results and discussion

Table 1 summarizes the synthesis conditions studied in this work. Fig. 1 shows the XRD patterns of the ZIFs obtained under ultrasound treatment (US) at 45 °C (ZIF-8 and ZIF-20) and 60 °C (ZIF-7 and ZIF-11) for several synthesis times and conventional solvothermal (ST) under conditions previously reported.[26] In the three cases studied in depth, all observed XRD

Table 1 Synthesis conditions

ZIF	Synthesis method	Synthesis temperature/°C	Synthesis time/h
ZIF-8	US	45	4, 6, 9
	ST	140	24
ZIF-7	US	60	3
ZIF-11	US	60	6, 9, 12
	ST	100	96[a]
ZIF-20	US	45	3, 6, 9, 12
	ST	65	72

[a] No pure ZIF-11 solid was obtained in these conditions (those reported by Park *et al.*[26]), see Fig. 1.

[a]*Department of Chemical and Environmental Engineering and Instituto de Nanociencia de Aragón (INA), Universidad de Zaragoza, 50018 Zaragoza, Spain. E-mail: coronas@unizar.es; Fax: +34 976 761879; Tel: +34 976 762471*

[b]*Instituto de Investigaciones en Catálisis y Petroquímica, INCAPE (FIQ, UNL-CONICET), Santiago del Estero 2829, 3000 Santa Fe, Argentina*

† Electronic supplementary information (ESI) available: Experimental details and additional results. See DOI: 10.1039/c2ce06382d

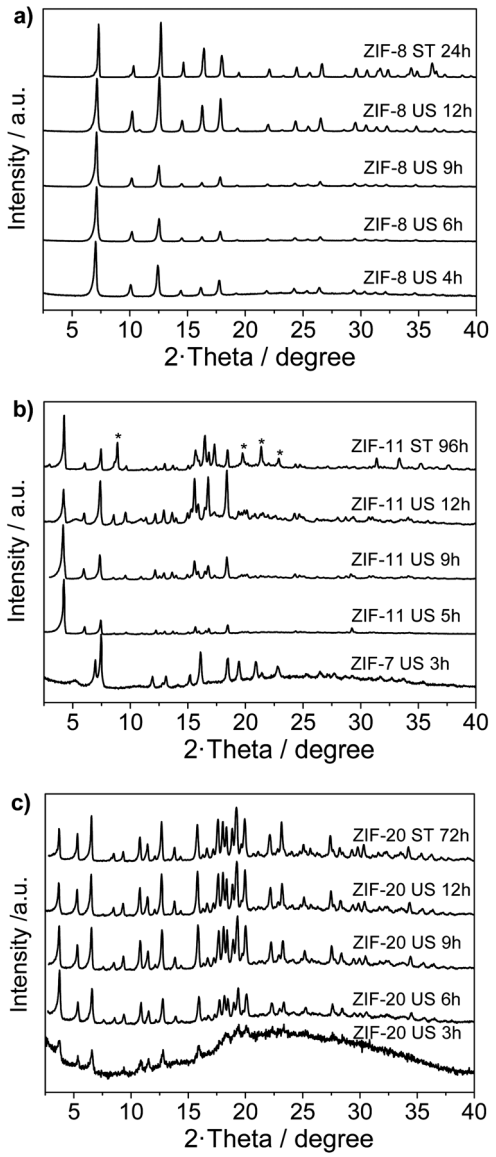

Fig. 1 X-Ray patterns of ZIF-8 (a), ZIF-11 (b) and ZIF-20 (c) obtained by sonocrystallization (US) after several times at 45 °C (ZIF-8 and ZIF-20) and 60 °C (ZIF-11) and using conventional solvothermal conditions (ST), see Table 1.

diffraction signals at 9 h match with the indexed diffractions of pure phases of ZIF-8, ZIF-11 and ZIF-20.[26,27]

Even though at synthesis times as short as 4–6 h the XRD appearance was good, the crystallinity was improved as a function of sonocrystallization time (Fig. 1 and 2). Moreover, in the case of ZIF-11 synthesis the phase obtained after 3 h was ZIF-7 (Fig. 1), while an unknown, dense phase (*) appeared at ST 96 h. This is the first time that the transformation from ZIF-7 to ZIF-11 is reported, even though similar MOF transformations have already been described as that of MIL-101 into MIL-53.[8] The synthesis time was considerably shorter for all of the ZIFs: from 24–72 h (ST) to 12 h or less (US). In addition, the synthesis temperature was reduced in all cases from those of the ST method of 140, 100 and 65 °C for ZIF-8, ZIF-11 and ZIF-20, respectively, to 45–60 °C. On the other hand, after treating the

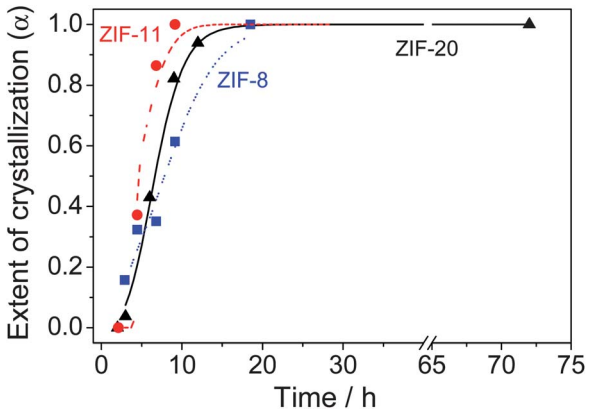

Fig. 2 Crystallization curves at 45–60 °C using US treatment. Reflections at 2θ values of 12.6°, 18.4° and 19.3° for ZIF-8, ZIF-11 and ZIF-20, respectively, were considered for the experimental extent of crystallization. Continuous lines were simulated with Gualtieri's model.[31]

mixture for the synthesis of ZIF-11 during 16 h at 45 °C, no solid was formed. However, after increasing the temperature of the ultrasound bath to 60 °C, turbidity appeared and pure ZIF-11 was recovered after 9 h (Fig. 1). This demonstrates the impact of the bath temperature on the kinetics of the reaction despite the extreme local conditions generated by the ultrasound cavitation itself.

Fig. 3 shows SEM images of the ZIFs synthesized by sonocrystallization. From these SEM images and those in Fig. S1†, cumulative crystal size distributions were obtained (Fig. 4). In general, as the sonocrystallization time increased, the crystal size also increased. However, from 3 to 6 h, an unexpected decrease

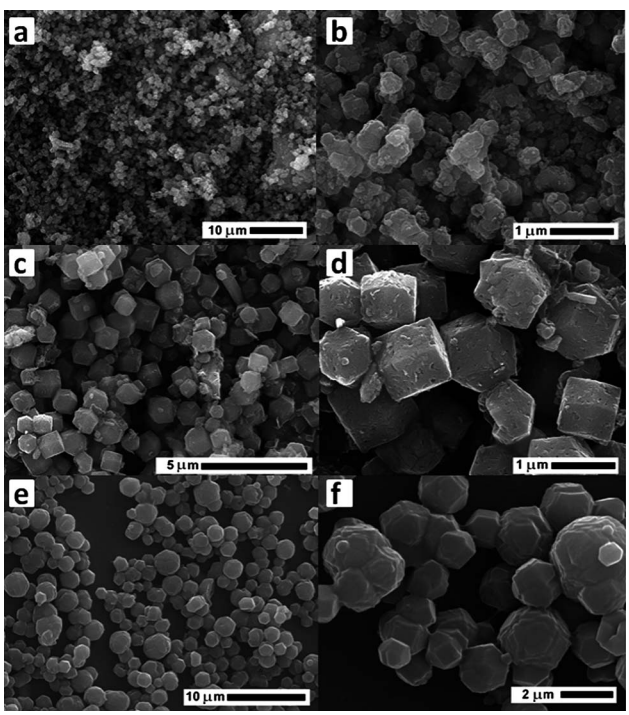

Fig. 3 SEM images after 9 h of sonocrystallization of ZIF-8 (a and b), ZIF-11 (c and d) and ZIF-20 (e and f).

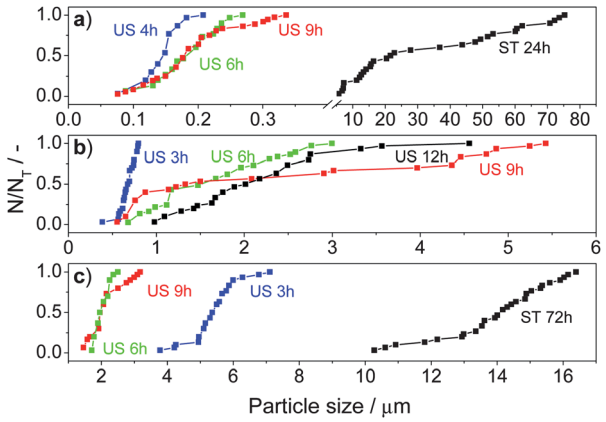

Fig. 4 Cumulative particle size distribution of ZIF-8 (a), ZIF-11 (ZIF-7 at 3 h) (b) and ZIF-20 (c) obtained by sonocrystallization (US) after several times at 45 °C (ZIF-8 and ZIF-20) and 60 °C (ZIF-11) and using conventional solvothermal conditions (ST), see Table 1. At $N/N_T = 0.5$, average particle sizes can be obtained from the curves: 0.15 μm (US 4 h), 0.18 μm (US 6 h), 0.18 μm (US 9 h) and 22 μm (ST 24 h) for ZIF-8; 0.68 μm (US 3 h), 1.5 μm (US 6 h), 1.3 μm (US 9 h) and 2.0 μm (US 12 h) for ZIF-11 (ZIF-7 at 3 h); and 5.4 μm (US 3 h), 2.0 μm (US 6 h), 2.0 μm (US 9 h) and 14 μm (ST 72 h) for ZIF-20.

of particle size is observed for ZIF-20 (Fig. 4c). This decrease of size runs parallel with an evident increase of crystallinity (Fig. 1c), so that a solid transformation from an initial amorphous phase to a denser ZIF-20 phase can be hypothesized. Moreover, Fig. 4b depicts a lower crystal size for ZIF-11 at 12 h than at 9 h, which can be explained by breaking at the high sonocrystallization time. In fact, in this case small particles are evident between large crystals (see SEM images at 9–12 h in Fig. 3 and S1†). Average crystal sizes were calculated at $N/N_T = 0.5$ and added to Fig. 4 caption highlighting that sonocrystallization was appropriated to obtain small crystal size ZIFs.

To summarize, smaller crystals (about one or two orders of magnitude smaller than those obtained by ST) with narrower size distribution (mainly for ZIF-8 and ZIF-20, see Fig. 4) were achieved by sonocrystallization when compared with conventional crystallization due to a promotion of the nucleation process in solution. As has recently been demonstrated for ZIF-20, the control of the crystal size may have an important influence on the material performance.[29]

Since the same dispersion compositions already reported for the ZIFs studied were used in this work and high crystallinity materials were achieved, no different empirical formulae to those already published are expected, *i.e.* $Zn(PhIM)_2 \cdot (H_2O)_3$, $Zn(MeIM)_2 \cdot (DMF) \cdot (H_2O)_3$, $Zn(PhIM)_2 \cdot (DEF)_{0.9}$ and $Zn(Pur)_2 \cdot (DMF)_{0.75} \cdot (H_2O)_{1.5}$ for ZIF-7, ZIF-8, ZIF-11 and ZIF-20, respectively.[26,27] Additionally, Fig. S2† depicts the comparison between TGA curves for typical ZIFs obtained under 9 h sonocrystallization and those corresponding to ZIFs obtained by conventional synthesis. In general, weight losses related to the decomposition of the ZIF structure were produced at a lower temperature for materials obtained by sonocrystallization. This may be due to their smaller crystal size that would mean a lower mass transfer resistance for the removal of degradation products. Finally, Fig. S3† shows the XRD stability of the activated materials obtained by sonocrystallization at 9 h. For this purpose, the materials were submitted to vacuum heating at 200 °C for 2 h. The results demonstrate that some of the materials (ZIF-20) have a poor thermal stability, while others (ZIF-8 and ZIF-11) remain relatively stable even though they showed clear damage in agreement with previous publications.[32]

Fig. 2 depicts the extent of crystallization (α) as a function of time. For ZIF-8 and ZIF-20 $\alpha = 1$ was considered for the material obtained by ST. In the case of ZIF-11 the pure phase was not obtained using the previously reported conditions, hence $\alpha = 1$ was considered for the sample synthesized during 12 h by US treatment. To gain an insight into the ZIF crystallization, the mathematical crystallization model developed by Gualtieri was applied.[31] This model was chosen because it allows nucleation and growth to be separated into two different processes and because it has already been applied to the crystallization of MOFs in conventional conditions, namely MOF-14 and HKUST-1 with good fittings.[33] In this model the extent of crystallization varies with time according to the following equation:

$$\propto = \frac{1 - e^{-(k_g t)^n}}{1 + e^{-(t-a)/b}}; k_n = \frac{1}{a} \quad (1)$$

where k_g is the rate of crystal growth, a and b are parameters related to nucleation and n is the dimension in which the growth takes place (1, 2 and 3 for needles, plates and 3D particles, respectively). For a better concordance between simulation and experimental results, the selected n was 3. k_n corresponds to the rate of nucleation. The values obtained for the parameters are listed in Table 2 and the simulated curves are shown in Fig. 2. k_n values are lower than (ZIF-8) or almost equal to (ZIF-11 and ZIF-20) k_g, in agreement with the fact that nucleation exerts an important influence on the ZIF crystallization, while $b > 0.33$ h suggests autocatalytic nucleation[31] for ZIF-8 and ZIF-20, as reported for MOF-14 and HKUST-1 below 100 °C[33] and for ZIF-8 below 135 °C.[34] ZIF-11 exhibits a lower b (0.11), which may be related to its higher sonocrystallization temperature (60 instead of 45 °C for the other two ZIFs) consistent with the predominance of heterogeneous over autocatalytic nucleation as reported for Na–X and Na–P zeolites at increasing temperatures.[31] On the other hand, in the case of zeolite A,[35] autocatalytic nucleation relates to all nuclei released from gel matrix during crystallization (including both precipitation and aging processes). Accordingly, sonocrystallization would promote autocatalytic nucleation at low temperature when the induction period of the conventional nucleation must be longer.

A difficult question to address that may arise here is the relation between the crystallization of ZIFs and that of zeolites having the same topologies, *i.e.* SOD topology for ZIF-8[26] and sodalite zeolites with different Si/Al ratios;[36] RHO topology for

Table 2 Kinetic parameters for the sonocrystallization of ZIF-8, ZIF-11 and ZIF-20 using Gualtieri's model[31]

ZIF	a/h	b/h	k_g/h^{-1}	k_n/h^{-1}
ZIF-8	8.07	3.75	0.30	0.12
ZIF-11	5.82	0.11	0.14	0.17
ZIF-20	5.21	2.41	0.18	0.19

ZIF-11[26] and zeolite rho;[37] and LTA topology for ZIF-20[27] and zeolites A and ITQ-29.[38] For instance, when LTA-type zeolites are considered, depending on the chemical composition a fast crystallization can be achieved for zeolite A with Si/Al atomic ratio around 2 at 90 °C for a few hours of hydrothermal treatment and without the need for an organic structure directing agent (OSDA),[39] while pure silica ITQ-29 is obtained at higher temperatures (135 °C) and much longer synthesis times (7 days) using an OSDA.[38] Thus for the same structure type the composition of the zeolite precursor dispersion plays a key role. From a general point of view, sonocrystallization accelerates crystal growth and this is true for the three ZIFs studied here in more detail. However, there are important differences in their synthesis conditions. First, 60 °C was the crystallization temperature for ZIF-11 instead of 45 °C for ZIF-8 and ZIF-20, and this temperature difference may support the different growth mechanism discussed about. Second, different ligands were used to obtain the ZIF phases: 2-methylimidazole (ZIF-8), benzylimidazole (ZIF-11) and purine (ZIF-20). Even though all these three compounds have obvious chemical similarities they are quite different, *e.g.* in molecular size. In consequence, distinct ZIF structures are obtained with different crystal growth kinetic parameters in more complex chemical systems than in the case of zeolites, where silicates and aluminosilicates species are common for a plethora of zeolites.

Conclusions

In conclusion, we have described the sonocrystallization of the zeolitic imidazolate frameworks ZIF-7, ZIF-8, ZIF-11 and ZIF-20. The pure crystals were achieved in shorter times (6–9 h) and at lower temperatures (45–60 °C) than with the conventional method. The crystals were smaller and had narrower particle size distribution. In addition, the application of the Gualtieri's model to simulate the extent of crystallization as a function of time allowed us to say that for ZIF-8 the nucleation rate controlled the crystallization process, while for ZIF-11 and ZIF-20 both growth and nucleation rates were similar.

Experimental

ZIFs were synthesized with the same reactant molar ratios as those reported in protocols for conventional solvothermal methods.[26,27] The synthesis of ZIF-20 was performed employing a solution with a Zn concentration of 0.05 mol L^{-1} and a Zn/organic linker ratio of 0.2. In a typical synthesis, $Zn(NO_3)_2 \cdot 6H_2O$ (74 mg, 0.25 mmol, Sigma-Aldrich) and purine (Pur) (150 mg, 1.25 mmol, Sigma-Aldrich) were dissolved in 5 mL of dimethylformamide (DMF) (Alfa Aesar). For ZIF-8, $Zn(NO_3)_2 \cdot 6H_2O$, 2-methylimidazole (MeIM) (Sigma-Aldrich) and DMF were mixed in 0.25 : 1.25 : 0.68 molar proportions. ZIF-11 was synthesized using $Zn(NO_3)_2 \cdot 6H_2O$, benzylimidazole (PhIM) (Sigma Aldrich) and diethylformamide (DEF) (Alfa Aesar) mixed in the following molar proportions: 0.25 : 1.25 : 0.68.

The prepared mixtures were agitated at room temperature for 30 min. The vessels were then immersed in an ultrasound bath containing water thermostatted at 45 or 60 °C and subjected to ultrasound radiation for different periods of time from 3 to 12 h. At low radiation time (3 h), ZIF-7 was obtained under ZIF-11 dispersion composition. The instrument (P Selecta Ultrasons) operated with a power of 110 W and a frequency of 47 kHz. After a few minutes of treatment, turbidity was observed in all of the solutions due to the precipitation of a solid of a yellowish-white color. These solids were separated by centrifugation at 10 000 rpm for 10 min, dispersed in DMF (ZIF-8 and ZIF-20) or DEF (ZIF-11), washed again with DMF or DEF and centrifuged twice. Finally, the solids were dried at room temperature for 1 h.

For comparison purposes the ZIFs were synthesized employing the conventional solvothermal methods[26,27] After 30 min of stirring, the mixtures were placed inside a 45 mL stainless steel Teflon-lined autoclave heated in an air convection oven at 140 °C for 1 day for ZIF-8, 100 °C for 4 days for ZIF-11, and 65 °C for 3 days for ZIF-20.

The amounts of solids obtained using ultrasound treatment were 3.8–7.3 mg (yield 2.9–5.6%), 1.1–7.5 mg (yield 0.4–2.9%) and 5.0–19.6 mg (yield 5.2–20.3%) for ZIF-8, ZIF-11 and ZIF-20 respectively. In the case of the synthesis carried out using the oven, the yields are higher, *i.e.* 48.4 and 26.0% for ZIF-8 and ZIF-20, respectively.

The formation of the different ZIF phases was confirmed by X-ray diffraction. The studies were performed at ambient temperature on a rotating anode diffractometer (D-Max Rigaku) using monochromatic CuKα radiation with $\lambda = 1.5418$ Å and a scanning rate of 0.03 ° s^{-1} between $2\theta = 2.5°$ and 40°. The XRD stability of the samples obtained after 9 h of sonocrystallization was studied. For this purpose, the materials were exchanged with methanol for 48 h (renewing the solvent every 12 h) at room temperature. The samples were then placed under vacuum at 200 °C for 2 h. Scanning electron microscopy (SEM) images of the ZIF particles were acquired with a JEOL JSM 6400 SEM instrument operating at 20 kV. All samples were coated with a thin film of Au. Thermogravimetric analyses were performed under N_2 atmosphere from 25 to 800 °C with a heating rate of 5 °C min^{-1} using a Mettler Toledo TGA/SDTA851e system.

Acknowledgements

Financial support (MAT2010-15870) and an FPU Program (B.S.) from the Spanish Science and Innovation Ministry are gratefully acknowledged. J.M.Z. acknowledges CONICET and the Universidad Nacional del Litoral of Argentina.

Notes and references

1 O. M. Yaghi, M. O'Keeffe, N. W. Ockwig, H. K. Chae, M. Eddaoudi and J. Kim, *Nature*, 2003, **423**, 705–714.
2 S. Kitagawa, R. Kitaura and S. Noro, *Angew. Chem., Int. Ed.*, 2004, **43**, 2334–2375.
3 G. Ferey, *Chem. Soc. Rev.*, 2008, **37**, 191–214.
4 C. B. Aakeroy, N. R. Champness and C. Janiak, *CrystEngComm*, 2010, **12**, 22–43.
5 Y. Yoo and H. K. Jeong, *Chem. Commun.*, 2008, 2441–2443.
6 J. S. Choi, W. J. Son, J. Kim and W. S. Ahn, *Microporous Mesoporous Mater.*, 2008, **116**, 727–731.
7 Y. Yoo, Z. P. Lai and H. K. Jeong, *Microporous Mesoporous Mater.*, 2009, **123**, 100–106.
8 N. A. Khan and S. H. Jhung, *Cryst. Growth Des.*, 2010, **10**, 1860–1865.
9 H. Bux, F. Y. Liang, Y. S. Li, J. Cravillon, M. Wiebcke and J. Caro, *J. Am. Chem. Soc.*, 2009, **131**, 16000–16001.
10 R. Ameloot, L. Stappers, J. Fransaer, L. Alaerts, B. F. Sels and D. E. De Vos, *Chem. Mater.*, 2009, **21**, 2580–2582.

11 W. J. Son, J. Kim and W. S. Ahn, *Chem. Commun.*, 2008, 6336–6338.
12 Z. Q. Li, L. G. Qiu, W. Wang, T. Xu, Y. Wu and X. Jiang, *Inorg. Chem. Commun.*, 2008, **11**, 1375–1377.
13 Z. Q. Li, L. G. Qiu, T. Xu, Y. Wu, W. Wang, Z. Y. Wu and X. Jiang, *Mater. Lett.*, 2009, **63**, 78–80.
14 E. Garcia-Perez, J. Gascon, V. Morales-Florez, J. M. Castillo, F. Kapteijn and S. Calero, *Langmuir*, 2009, **25**, 1725–1731.
15 D. Farrusseng, S. Aguado and C. Pinel, *Angew. Chem., Int. Ed.*, 2009, **48**, 7502–7513.
16 B. Zornoza, A. Martinez-Joaristi, P. Serra-Crespo, C. Tellez, J. Coronas, J. Gascon and F. Kapteijn, *Chem. Commun.*, 2011, **47**, 9522–9524.
17 D. Y. Hong, Y. K. Hwang, C. Serre, G. Ferey and J. S. Chang, *Adv. Funct. Mater.*, 2009, **19**, 1537–1552.
18 Y. Takashima, V. M. Martinez, S. Furukawa, M. Kondo, S. Shimomura, H. Uehara, M. Nakahama, K. Sugimoto and S. Kitagawa, *Nat. Commun.*, 2011, **2**, 1–8.
19 P. Horcajada, C. Serre, G. Maurin, N. A. Ramsahye, F. Balas, M. Vallet-Regi, M. Sebban, F. Taulelle and G. Ferey, *J. Am. Chem. Soc.*, 2008, **130**, 6774–6780.
20 K. S. Suslick, *Science*, 1990, **247**, 1439–1445.
21 K. S. Suslick, T. Hyeon, M. M. Fang and A. A. Cichowlas, *Mater. Sci. Eng., A*, 1995, **204**, 186–192.
22 J. Park, B. C. Kim, S. S. Park and H. C. Park, *J. Mater. Sci. Lett.*, 2001, **20**, 531–533.
23 O. Andac, M. Tather, A. Sirkecioglu, I. Ece and A. Erdem-Senatalar, *Microporous Mesoporous Mater.*, 2005, **79**, 225–233.
24 B. Y. Wang, H. M. Wu, Z. Y. Yuan, N. Li and S. H. Xiang, *Ultrason. Sonochem.*, 2008, **15**, 334–338.
25 E. Haque, N. A. Khan, J. H. Park and S. H. Jhung, *Chem.–Eur. J.*, 2010, **16**, 1046–1052.
26 K. S. Park, Z. Ni, A. P. Cote, J. Y. Choi, R. D. Huang, F. J. Uribe-Romo, H. K. Chae, M. O'Keeffe and O. M. Yaghi, *Proc. Natl. Acad. Sci. U. S. A.*, 2006, **103**, 10186–10191.
27 H. Hayashi, A. P. Cote, H. Furukawa, M. O'Keeffe and O. M. Yaghi, *Nat. Mater.*, 2007, **6**, 501–506.
28 B. Zornoza, P. Gorgojo, C. Casado, C. Tellez and J. Coronas, *Desalin. Water Treat.*, 2011, **27**, 42–47.
29 B. Seoane, J. M. Zamaro, C. Tellez and J. Coronas, *RSC Adv.*, 2011, **1**, 917–922.
30 B. Zornoza, B. Seoane, J. M. Zamaro, C. Téllez and J. Coronas, *ChemPhysChem*, 2011, **12**, 2781–2785.
31 A. F. Gualtieri, *Phys. Chem. Miner.*, 2001, **28**, 719–728.
32 Y. Pan, Y. Liu, G. Zeng, L. Zhao and Z. Lai, *Chem. Commun.*, 2011, **47**, 2071–2073.
33 F. Millange, R. El Osta, M. E. Medina and R. I. Walton, *CrystEngComm*, 2011, **13**, 103–108.
34 J. Cravillon, C. A. Schroder, H. Bux, A. Rothkirch, J. Caro and M. Wiebcke, *CrystEngComm*, 2012, **14**, 492–498.
35 A. Palcic, J. Bronic, D. Brlek and B. Subotic, *CrystEngComm*, 2011, **13**, 1215–1220.
36 S. B. Hong, M. A. Camblor and M. E. Davis, *J. Am. Chem. Soc.*, 1997, **119**, 761–770.
37 H. E. Robson, D. P. Shoemaker, R. A. Ogilvie and P. C. Manor, *Adv. Chem. Ser.*, 1973, 106–115.
38 A. Corma, F. Rey, J. Rius, M. J. Sabater and S. Valencia, *Nature*, 2004, **431**, 287–290.
39 O. de la Iglesia, R. Mallada, M. Menéndez and J. Coronas, *Chem. Eng. J.*, 2007, **131**, 35–39.